Temperature - and Injection-Dependent Lifetime Spectroscopy

Derek Greer
Benjamin Kostreva
Walter Schlosser
Matthew Mahaffey

April 14, 2015

Abstract

The goal of temperature and injection dependent lifetime spectroscopy (TIDLS) is to accurately identify defects in a given semiconductor material. In order to accomplish this goal, TIDLS utilizes the Shockley-Read-Hall (SRH) model for the charge carrier lifetime (τ_{SRH}), which is characterized in terms of the symmetry factor k, the charge carrier capture time constant τ_{n_0,p_0}, and the energy of the defect E_t. k is a ratio of the capture cross-sections σ_n and σ_p. For varying temperatures and excess carrier concentrations ($\Delta_{\mathrm{n,p}}$), the charge carrier lifetime τ_{SRH} is measured. Manipulating both temperature and injection dependence parameters allows us to accurately identify defects in a semiconductor. We use a non-linear least-squares regression to fit the charge carrier lifetime data to the Shockley-Read-Hall model in order to create solution spaces for both the charge carrier time constant and the symmetry factor in terms of the defect energy ($\tau_{\mathrm{n_0,p_0}}(E_t)$ and $k(E_t)$). By superimposing these solution spaces for varying temperatures, we find the defect energies E_t, and thus identify the defects within a semiconductor sample. Data was collected for an intentionally iron contaminated boron doped silicon sample, and the defect properties for iron are successfully extracted.

1 Introduction

This section reviews temperature- and injection-dependent lifetime spectroscopy as a method for analyzing defects in semiconductors. TIDLS can effectively disambiguate defects due to its use of both injection-dependent lifetime spectroscopy (IDLS) and temperature-dependent lifetime spectroscopy (TDLS) [1]. The method also relies on the Shockley-Read-Hall (SRH) statistics of recombination for charge carriers, due to the presence of one or more electrically active impurities with an activation energy that exists in the band gap of any semiconductor [2]. Electrically active defects causing recombination may limit efficiency in solar cells, even in dilute concentrations [3, 4].

The effective time (τ_{eff}) required for a charge carrier to recombine to its lowest energy state due to impurities can be derived with the framework of SRH statistics [5]. An analysis shows that the charge carrier lifetimes depend on the excess concentration of minority carriers above the thermal equilibrium value for the material [6]. Therefore, analyzing the minority carrier lifetime is an effective way to assess the quality of semiconductors [7]. The minority carrier lifetime can be determined from recombination processes, such as SRH recombination, radiative recombination, and Auger recombination [8, 9]. The TIDLS method isolates SRH recombination from the other forms of recombination. The proposed method is useful because recombination processes depend upon temperature [10, 11]. Of particular note is the fact that SRH statistics utilized in TIDLS are for point-defect recombination and cannot be applied to recombination via precipitates [12]. Data for lifetime versus excess minority carrier density at different temperatures can be collected and analyzed in order to provide an approximation of the impurity energy level in the band gap. A single impurity can be resolved using this approximation, and an expansion of the model may also allow resolution of multiple impurities [13].

Our work focuses on the development of a software package, which will implement the TIDLS method of defect identification through a nonlinear least-squares fit. Initially, the method is debugged by generating simulated data with a specified defect level, and then running the analysis to extract back the defect level. After calibration and debugging, we apply the nonlinear regression to empirically derived data and extract the defect characteristics unique to the data set taken from an intentionally iron contaminated set of boron doped silicon semiconductor wafers.

2 Background

In the analysis of semiconductors, the equilibrium concentrations of charge carriers are vital to understanding the material's properties [14]. From statistical mechanics, the densities of electrons and holes are [15]:

$$n = \int_{E_c}^{\infty} D_c(E) f(E) dE,\ p = \int_{-\infty}^{E_v} D_v(E) f(E) dE \tag{1}$$

where n and p are the electron and hole concentrations, $D_{c,v}(E)$ are the density of states functions, $f(E)$ is the Fermi-Dirac distribution function, and E_c and E_v are the conduction and valence band energies respectively.

The Fermi-Dirac distribution function is given by [15]:

$$f(E) = \left(1 + \exp\left(\frac{E - E_F}{k_B\ T}\right)\right)^{-1} \tag{2}$$

When the Fermi energy E_F differs from the band edges by several times $k_B T$, the distribution in equation (2) can be reduced since the constant 1 is negligible compared to the exponential term. The integration in equation (1) becomes much easier to evaluate and results in closed form expressions for the electron and hole concentrations [16]:

$$n_0 = N_C\ \exp\left(-\frac{E_c - E_F}{k_B\ T}\right); p_0 = N_V\ \exp\left(-\frac{E_F - E_v}{k_B\ T}\right) \tag{3}$$

In equation (3), N_C and N_V are the effective densities of states for electrons and holes respectively. A useful result is derived from the law of mass action applied to the carriers, which results in [16]:

$$n_i^2 = n_0\ p_0 = N_C\ N_V\ \exp\left(-\frac{E_{gap}}{k_B\ T}\right) \tag{4}$$

Equation (4) shows that n_i, the intrinsic concentration, is a material property which depends only on the band gap energy, E_{gap}, which is short hand for $E_c - E_v$.

With respect to doping, equilibrium concentrations differ from those given in Equation (3). The concentrations of carriers depend on the temperature range in question. The three ranges of temperatures of importance are shown in Table 1.

Table 1: The three regions of interest for temperature, and their effect on the equilibrium concentration of carriers [16].

0 - 150 K	freeze-out	$p_0(T) < N_{A,D}$
150 - 500 K	impurity depletion	$p_0(T) = N_{A,D}$
$>$ 500 K	intrinsic conduction	$p_0(T) > N_{A,D}$

$N_{A,D}$ is the concentration of dopant (acceptors and donors, respectively) atoms in the material.

Like the equilibrium concentrations for the intrinsic carriers, the concentration of ionized dopant atoms depends on temperature. Only the ionized atoms contribute to the excess hole or electron concentrations. In the freeze-out region, the equilibrium concentration of ionized dopant atoms is negligible, and the effective carrier concentration is much smaller than the actual dopant concentration. In the impurity depletion region, a negligible amount of unionized dopant atoms is left, and the carrier concentration is therefore approximately equal to the dopant concentration. Lastly, in the intrinsic conduction range, the equilibrium concentration of the intrinsic carriers found in Equation (3) dominates the dopant atoms, and the effective concentration is therefore much larger than the dopant concentration.

Statistical methods allow the derivation of the ionized dopant concentrations in terms of the temperature and result in an expression for the fraction of the total atoms ionized [16].

$$f_{\mathrm{A}}(T) = \left(1 + 2\,\exp\left(-\frac{E_{\mathrm{F}} - E_{\mathrm{A}}}{k_{\mathrm{B}}\,T}\right)\right)^{-1} \tag{5}$$

The value E_{A} in Equation (5) refers to the energy level that the dopant atom adds inside of the band gap. A more complete definition of the carrier concentration is then found to be [16]

$$p_0(T) = \begin{cases} f_{\mathrm{A}}(T) N_{\mathrm{A}} & T < 350\,^{\circ}\mathrm{C} \\ \frac{1}{2} * \left(N_{\mathrm{A}} + \sqrt{N_{\mathrm{A}}^2 + 4 n_{\mathrm{i}}(T)^2}\right) & T \geq 350\,^{\circ}\mathrm{C} \end{cases} \tag{6}$$

where the definition for $T \geq 350\,^{\circ}\mathrm{C}$ is derived through use of the definition of intrinsic concentration in Equation (4).

In the event that the concentration of electrons or holes is above or below the equilibrium value, there is a net rate of change in the excess carrier density, $\Delta n = n - n_0$, which is the result of a difference between the rate carriers are generated, G_0, and the rate that electrons are recombining with holes, R_0. This net rate of change results in the excess carrier density approaching zero, and thus the carrier concentrations approaching equilibrium. This rate of change is quantified through the equations below [16].

$$\frac{\partial \Delta n(t)}{\partial t} = -U(\Delta n(t), n_0, p_0) \tag{7}$$

Equation (7) defines the rate of change in the excess carrier density as a function U which depends on the current excess, as well as the equilibrium values. The dependence of the rate of change of the excess density on its current value implies an exponential decay. The time constant of this decay is referred to as the recombination lifetime and is generally defined as [16]:

$$\tau(\Delta n, n_0, p_0) = \frac{\Delta n}{U(\Delta n, n_0, p_0)} \tag{8}$$

In semiconductors, there are various mechanisms through which a carrier can undergo recombination. These different mechanisms happen independently of each other, and therefore each have an associated recombination rate. The effective rate is then the linear sum of these,

$$U_{\mathrm{eff}} = \sum_v U_v \tag{9}$$

where the sum is understood to be over all mechanisms in question. It follows from Equations (8) and (9) that the effective lifetime can be found by

$$\frac{1}{\tau_{\text{eff}}} = \sum_{v} \frac{1}{\tau_v} \tag{10}$$

In the case of TIDLS, the effective lifetime is dominated by recombination through a defect level. When a defect is present in the material, it provides another available energy in the band gap. The carriers then transition from a band edge to the defect level, and then recombine. The mathematics of this mechanism are referred to as Shockley Read Hall theory, and derive the lifetime associated with recombination through a defect. The rates for carrier capture and emission are shown in SRH theory to obey fairly simple relations shown in the equations [16]

$$c_{\text{p,n}} = (\sigma_{\text{p,n}}\ v_{\text{th}})\ (\text{p,n}) \tag{11}$$

$$e_{\text{p,n}} = (\sigma_{\text{p,n}}\ v_{\text{th}})\ (\text{p}_1, \text{n}_1) \tag{12}$$

Equation (11) introduces σ_{n} and σ_{p}, which are constants referred to as the capture cross sections for electrons and holes, respectively. The value of v_{th} is the thermal velocity of the carriers in the material. In equation (12), the densities n_1 and p_1 are expressions that result from the SRH derivation. Their expressions are

$$n_1 = N_{\text{C}}\ \exp\left(-\frac{E_{\text{c}} - E_t}{k_{\text{B}}\ T}\right)\ ,\ p_1 = N_{\text{V}}\ \exp\left(-\frac{E_t - E_v}{k_{\text{B}}\ T}\right) \tag{13}$$

where E_{t} is the energy of the defect in the band gap. The rate of recombination is written using these rates for emission and capture, and the SRH derivation ends in an expression for the lifetime [16]:

$$\tau_{SRH} = \frac{\tau_{\text{n}_0}(p_0 + p_1 + \Delta n) + \tau_{\text{p}_0}(n_0 + n_1 + \Delta n)}{p_0 + n_0 + \Delta n} \tag{14}$$

of this mechanism where τ_{n_0} and τ_{p_0} are constants referred to as the effective lifetimes of electrons and holes, respectively. The expression for these constants is given in Equation (15) [16].

$$\tau_{n_0,p_0} = (N_{\text{t}}\ \sigma_{\text{n,p}}\ v_{\text{th}})^{-1} \tag{15}$$

In Equation (15), N_{t} is the concentration of defect atoms, while $\sigma_{\text{n,p}}$ again refers to the capture cross sections. Equation 14 can be manipulated in such a way so as to extract unique characteristics specific to individual defects.

The defect parameter k is defined as a symmetry factor. The extent of capture asymmetry is a characteristic feature of the defect state. k is defined in the following manner: [16]

$$k = \frac{\sigma_{\text{n}}}{\sigma_{\text{p}}} = \frac{\tau_{\text{p}_0}}{\tau_{\text{n}_0}} \tag{16}$$

This symmetry factor depends only on the defect structure - not on the absolute quantities N_t & $\sigma_\mathrm{n,p}$. This implies that k is a *relative* defect parameter like the energy level E_t. By substitution the Shockley-Read-Hall equation becomes [16]

$$\tau_\mathrm{SRH} = \boldsymbol{\tau_{n_0}} \left[\frac{p_0 + N_V \, e^{\dfrac{-(\boldsymbol{E}_\mathrm{t} - E_\mathrm{v})}{k_\mathrm{B}T}} + \Delta n}{p_0 + n_0 + \Delta n} \; + \; \boldsymbol{k} \frac{n_0 + N_\mathrm{c} \, e^{\dfrac{-(E_\mathrm{c} - \boldsymbol{E}_\mathrm{t})}{k_\mathrm{B}T}} + \Delta n}{p_0 + n_0 + \Delta n} \right] \tag{17}$$

The parameters in bold font are used as free parameters for the nonlinear least squares fit. By assigning values to E_t throughout the band gap, it is possible to build two defect parameters solution spaces - $\tau_{\mathrm{n_0,p_0}}(E_\mathrm{t})$ & $k(E_\mathrm{t})$. Refer to figures 2a and 2b for examples of these defect parameter solution spaces.

This functional form of the SRH lifetime includes the general dependence of the phenomenon on injection level, doping concentration, defect parameters, and temperature. It also illustrates the trends associated with changes in the parameters. Any variation of the absolute defect parameters results in a vertical shift of the lifetime curves. However, changes in the relative defect parameters will have an influence on the shapes of the curves. Only E_t and k can be determined exclusively, while the determination of N_t & $\sigma_\mathrm{n,p}$ requires an additional spectroscopic method to separate the two parameters. This method is discussed in greater detail in the theory and procedure section.

3 Theory and Procedure

For the analysis of defects to proceed, it is necessary to remove unknown values from the lifetime in (14). The ratio of cross sections (also called the symmetry factor), k, is introduced and is given by (16) where σ refers to the respective capture cross section. Introducing this into the SRH lifetime results in a slightly modified expression.

$$\tau_{\mathrm{SRH}} = \tau_{\mathrm{n_0}} \left(\frac{p_0 + p_1 + \Delta n}{p_0 + n_0 + \Delta n} + k \frac{n_0 + n_1 + \Delta n}{p_0 + n_0 + \Delta n} \right) \tag{18}$$

The substitution of k results in expression (18) since by the definitions of the effective lifetimes in (15) the relation $k = \tau_{\mathrm{p_0}}/\tau_{\mathrm{n_0}}$ holds.

The defining value for the defect is E_t, the energy level provided in the band gap. This value is located in (18) through the dependency on n_1 and p_1. Equation (13) shows how the defect energy determines these two values. The full functional dependency with each expression substituted in is given in equation (17). To extract E_t from collected data, equation (18) can be fit to the points and the E_t which provides the best fit is the defect energy present. The parameters $\tau_{\mathrm{n_0}}$ and k are selected as fitting coefficients in order to remove the dependencies hidden in these two terms. Equations (15) and (16) reveal that the dependency on the cross sections, σ, the amount of defect atoms, N_t, and the thermal velocity, v_{th}, is removed by allowing $\tau_{\mathrm{n_0}}$ and k to change as needed during the fitting process. Assuming the properties of the semiconductor are known, which includes band energies and doping concentration, the remaining dependencies in equation (18) include temperature, T, injection level, Δn, and defect energy, E_t.

Data for the lifetime versus the injection level is collected at multiple temperatures in order for the fitting process to identify the defect energy. A temperature is selected, the value of E_t is selected near the bottom of the band gap, and $\tau_{\mathrm{n_0}}$ and k are used as free parameters to find a fit and associated χ^2 value. The value set for E_t is then incremented towards the top of the band gap, and the fit repeated. After iterating through the entire band gap, the temperature is changed and the process is repeated for the data at this new temperature. The amount that E_t is incremented between fits determines the resolution of the method, since a smaller increment results in testing more values of E_t which will then come closer to the actual value. Figure 1 is a flowchart which presents the entire process.

After fitting data for many values of E_t, the relationship between the calculated values for $\tau_{\mathrm{n_0}}$ and k from fitting and the corresponding E_t is plotted to display the results at different temperatures. These are referred to as the two solution spaces that the fitting process provides. Example solution spaces are shown in Figures 2a & 2b. The point of interest in the solution spaces is where the curves for $\tau_{\mathrm{n_0}}(E_t)$ or $k(E_t)$ at different temperatures intersect. It is expected that when the correct value of E_t is selected during iteration, the correct values for $\tau_{\mathrm{n_0}}$ and k will be found by the fitting algorithm, regardless of the temperature. This temperature independence of $\tau_{\mathrm{n_0}}$ and k at the correct value of E_t means that the value of E_t at the intersection in the solution spaces is the actual defect energy. It is important to note that this method of extracting the defect energy inherently assumes that the true functional forms of $\tau_{\mathrm{n_0}}$ and k are temperature independent. It is this assumption that allows us to select the intersection as the correct defect energy.

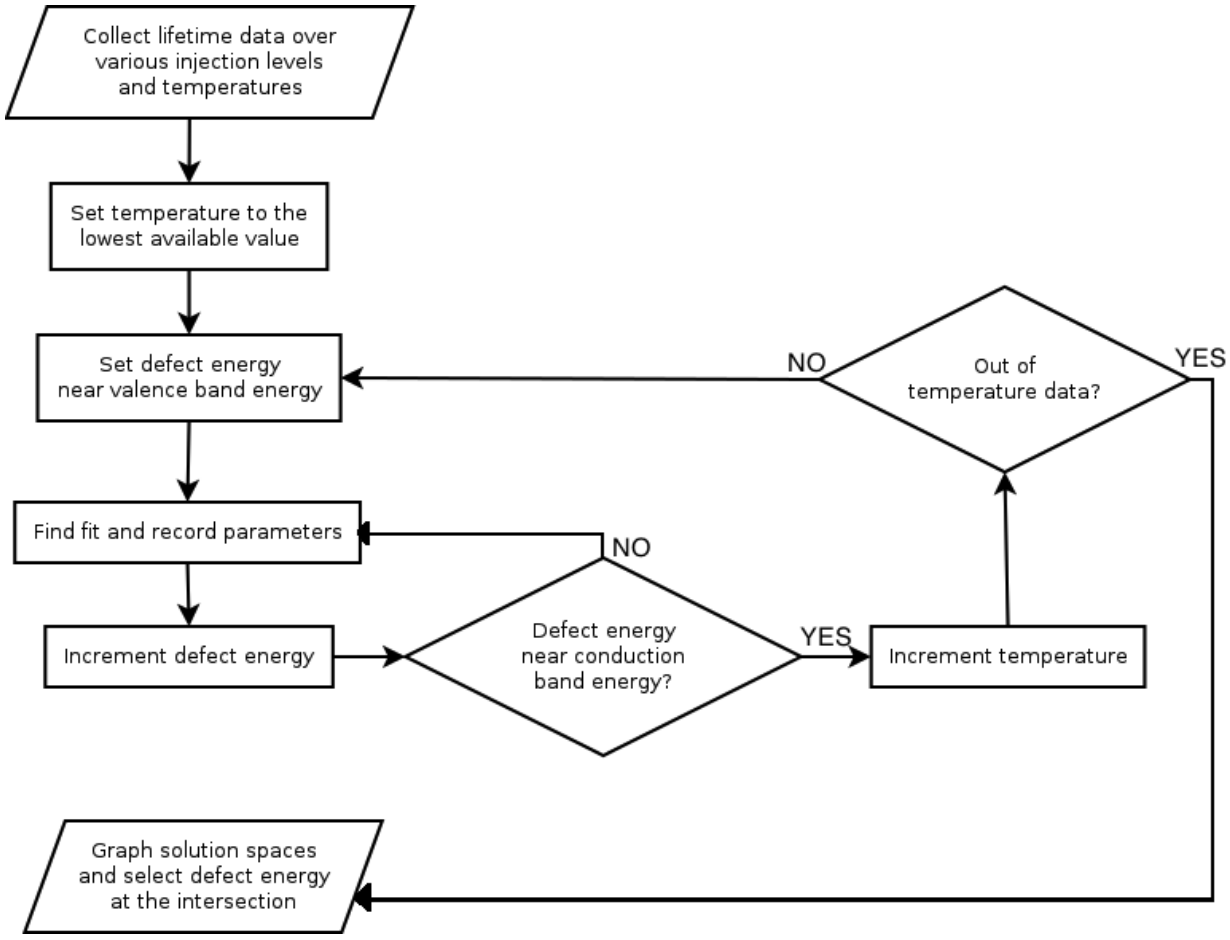

Figure 1: A flowchart which represents the entire process for identifying the defect energy present from raw data is shown.

Fe contaminated B-doped Si

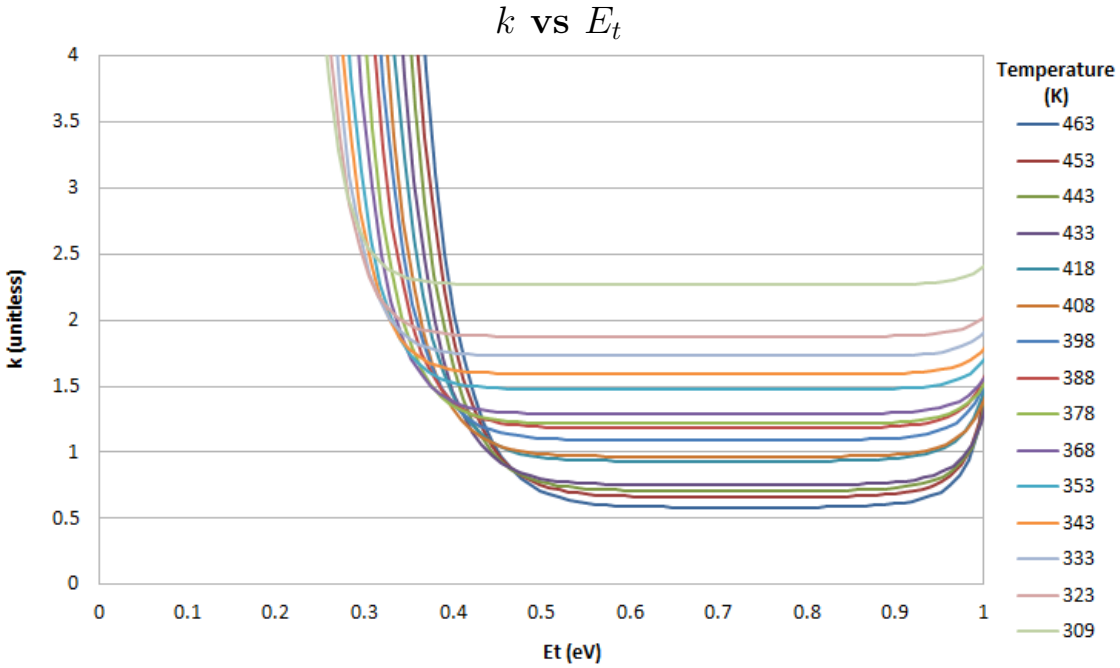

(a) The solution space for k is shown.

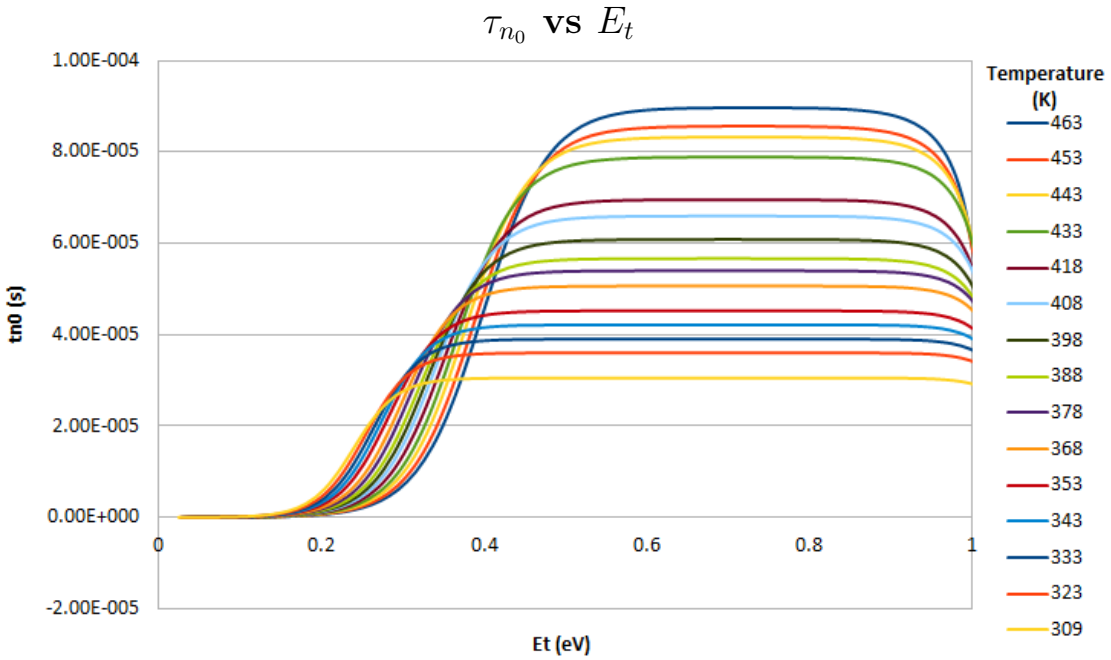

(b) The solution space for τ_{n_0} is shown.

Figure 2: Solution spaces for an iron contaminated boron doped silicon sample are shown.

4 Results

Figures 3a and 3b display the simulated SRH lifetime τ_{SRH} data as well as the effective lifetime τ_{eff} data collected from the real sample. The simulated data was generated using generic defect concentrations, as well as a defect enery level of 0.26 eV. The sample in question is an intentionally iron contaminated boron doped silicon wafer, and data was collected using the tool provided by Sinton Instruments. In comparison of each lifetime plot, it is apparent that the real data contains lifetime contributions from Auger and radiative recombination, but since the wafer is intentionally contaminated, the SRH lifetime dominates in the curvature. It should be noted that for a sample with unknown contamination levels, extraction of the SRH lifetime from the effective may be necessary if the defect concentration is much lower. The TIDLS software was run on both data sets shown in Figure 3 in order to provide the theoretical solution spaces as well as the experimental.

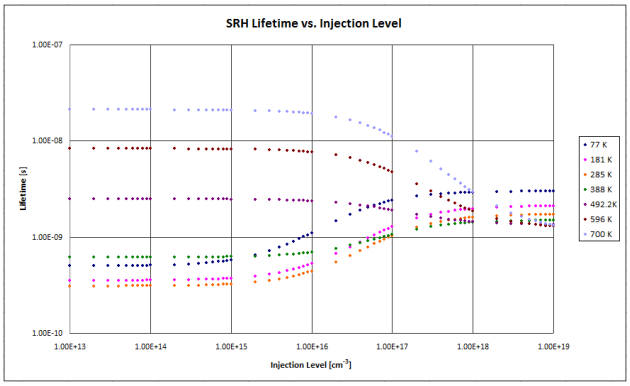

(a) Generated data for the SRH lifetime τ_{SRH} in terms of injection level Δn at different temperatures is shown.

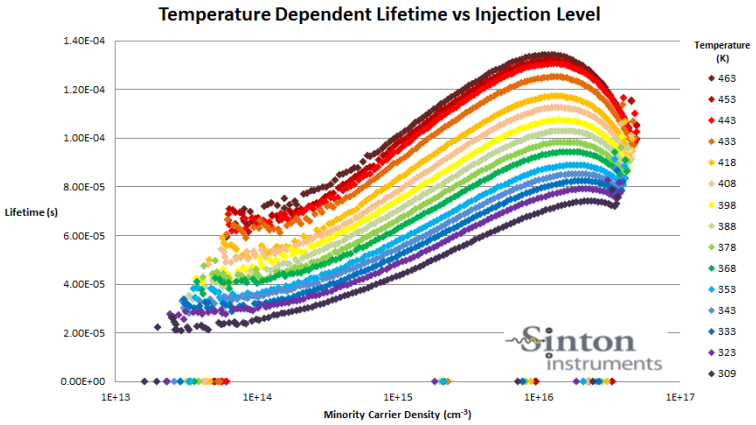

(b) Data for the bulk lifetime τ_{eff} in terms of injection level Δn at different temperatures is shown for an Fe contaminated sample.

Figure 3: SRH lifetime τ_{SRH} data generated using the functional form of (14) with generic defect parameters is shown along with the collected bulk lifetime τ_{eff} data for the Fe contaminated sample. Data collection was provided by Sinton Instruments.

Figures 4 and 5 display solution spaces for k and τ_{n_0} output by the TIDLS software after analyzing the lifetime data. In each figure, the simulated results are shown on the left with the experimental results displayed on the right. In 4a and 5a, there is a well defined intersection between all curves as expected since the simulated data contains little to no error. In both figures, the intersection lies near 0.26 eV on the horizontal axis which is in agreement with the value used to generate the data and is consistent with the literature for the dominant defect. This result confirms that the implementation of the fitting algorithm is correct and may be used for analysis of the experimental data. Figures 4b and 5b display the results of processing the experimental data. These plots exhibit diffuse intersections which span a range of possible values for the defect energy which is expected due to experimental error.

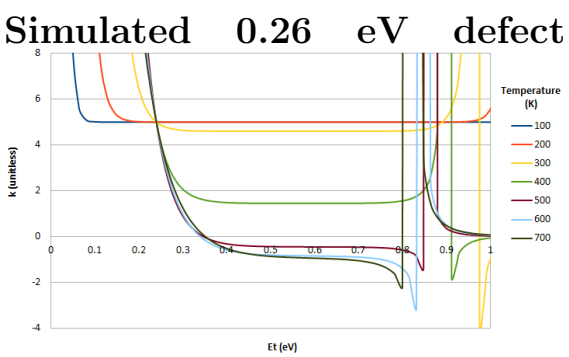

(a) k space for simulated data is shown.

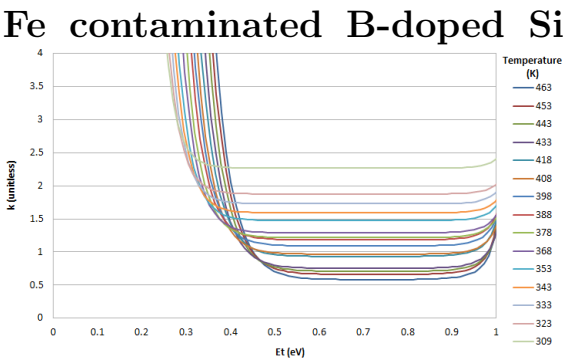

(b) k space for an Fe contaminated sample is shown.

Figure 4: The k solution spaces for simulated data and an Fe contaminated sample are shown for comparison.

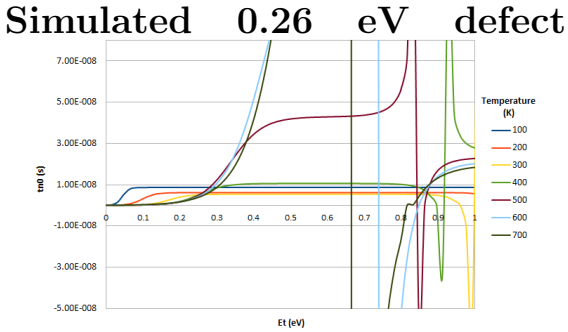

(a) τ_{n_0} space for simulated data is shown.

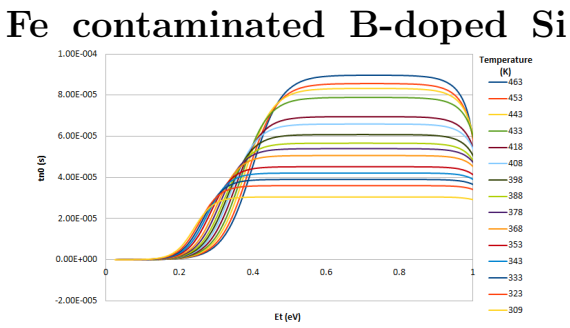

(b) τ_{n_0} space for an Fe contaminated sample is shown.

Figure 5: The τ_{n_0} solution spaces for simulated data and an Fe contaminated sample are shown for comparison.

Comparison of the plots in figures 4 and 5 provides strong evidence that the theoretical solution space curvatures agree with experiment. With respect to the experimental k solution space in figure 4b, the span of possible defect energy values is approximately 0.3 to 0.45 eV. The span of possible k values is approximately 1.6 to 2.2. The iron defect is characterized in literature by its k value, which is in agreement with the result provided by figure 4b [16]. The τ_{n_0} experimental solution space in figure 5b provides a range of defect energy values consistent with the k space, approximately 0.27 to 0.45 eV from leftmost intersection to rightmost. The τ_{n_0} defect property for iron is less studied, and instead the solution space is used to cross check the apparent defect energy range with the k space. Agreement between the two spaces provides evidence that the TIDLS method has the potential to correctly extract the defect properties. Proposed methods for improving the TIDLS algorithm and analysis of its flaws are discussed in the Future Research section.

4.1 Cost Analysis

Table 2 shows a breakdown of the costs associated with the TIDLS project. The majority of the project is focused around software development and there are very few costs involved. Several contacts from around the world are sending us silicon samples in order to acquire lifetime data and run our TIDLS defect analysis on their samples. Due to remote locations of our collaborators, there will be shipping costs associated with transporting the samples back to their owners' locations. These locations include France, Australia, UK, Arizona, and Massachusetts. The labor costs for this project involve software development, time spent on data acquisition, and any overhead associated with the project. The capital requirements of the project (such as the apparatus used to acquire lifetime data) are not included in this cost analysis. There are no other costs, as all of our samples are provided to us from outside sources and the software development will be done completely in C++.

Table 2: Cost analysis for the TIDLS project

Item	**Unit Cost**	**Quantity**	**Unit**	**Cost**
Shipping - International	\$54.55	6	ea	327.30
Shipping - Domestic	\$6.45	5	ea	32.25
Labor - Software Development	\$11.00	70	hr	770.00
Labor - Data Acquisition	\$19.00	10	hr	190.00
Overhead - 50% of Labor	–	–	–	480.00
Total Cost				**1799.55**

The labor associated with the data acquisition in table 2 represents the estimated time spent at Sinton Instruments using their lifetime tester. This work will be performed by a single team member and is billed according to that team member's current pay rate. We approximate a contribution of 70 hours in software development between each of the team members working on this aspect of the project. The pay rate is reflective of the current pay rate received by the team members involved in software development.

4.2 Facilities, Equipment, and Other Resources

- **National Renewable Energy Laboratory (NREL)**
  National Renewable Energy Laboratory in Golden, Colorado, is providing the use of a photoluminescence spectroscopy device to support defect analysis in real samples.

- **Sinton Instruments**
  Sinton Instruments in Boulder, Colorado is providing the use of a WCT-120 to determine lifetimes empirically.

- **Intentionally Contaminated Silicon Wafers**
  A silicon wafer manufacturer in Lyon, France, has contributed a set of intentionally contaminated silicon wafers. These wafers will serve as experimental controls during software calibration.

5 Further Research

As discussed in the Theory and Procedure section, the TIDLS method for extracting defect energy levels relies on temperature independence in the fitting parameters. The simulated solution spaces in figures 4a and 5a display well defined intersections at the correct defect energy since the two parameters, τ_{n_0} and k, were simulated with no temperature dependence. However, the temperature dependence of τ_{n_0} is known and given by equation (15). The fact that the real value of this parameter is not temperature independent means a well defined intersection in the τ_{n_0} solution space is not possible. The parameter k is also accepted to be temperature dependent, though the functional dependence is not as well known since the dependence of the capture cross sections on temperature is not well studied. Since the experimental data was from an intentionally iron-contaminated sample, the correct horizontal position for the intersection in the solution spaces is known, and so the temperature dependence of the parameters can be extracted. The results of this extraction are shown in figure 6.

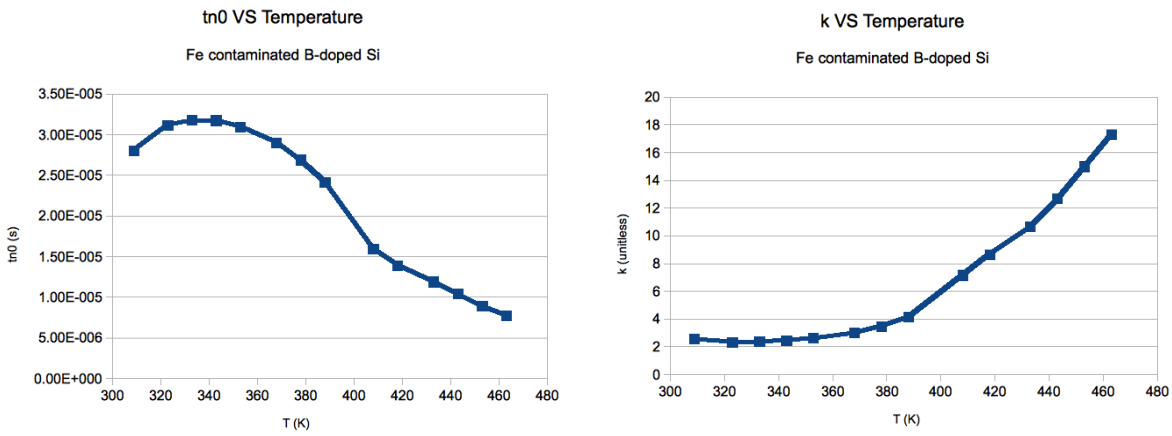

(a) The apparent temperature dependence of the parameter τ_{n_0} is shown.

(b) The apparent temperature dependence of the parameter k is shown.

Figure 6: Temperature dependence of the two fitting parameters was isolated from the solution spaces and is shown above.

In order to reduce the diffuse intersection ranges displayed in figures 4b and 5b, the temperature dependence of the fitting parameters must be reduced. This may be accomplished through new approximations for the functional form of each parameter, or by fitting a different set of parameters which is known to exhibit little to no temperature dependence. Any advances in controlling this dependence will improve the TIDLS method for determining defect properties.

6 Conclusion

TIDLS is a promising method for determining defects present in semiconductor materials. It is shown in figures 4 and 5 that the theory behind the method produces qualitatively the same curvature as the experimental data. In addition, the experimental data provided a range for the k value for an iron defect that is consistent with accepted values, 1.6 to 2.2. Agreement in the defect energy range between the experimental k and τ_{n_0} provides evidence that the range of possible values, 0.3 to 0.45 eV, contains the correct value for the iron defect. The cause of the diffuse intersections in the experimental solution spaces is due to experimental error, as well as a temperature dependence in each of the solution parameters. Approximation methods for the parameter temperature dependencies or selecting different parameters with a smaller temperature dependence will allow the method to produce more exact results in the future. As it stands, TIDLS can successfully analyze lifetime data and provide a range for the possible defect properties and allow either identification of the defect or further study of an intentional defect's behavior.

References

[1] D. Macdonald and A. Cuevas, "Validity of simplified Shockley-Read-Hall statistics for modeling carrier lifetimes in crystalline silicon," Phys. Rev. B **67**, 075203 (2003).

[2] W. Shockley and W.T. Read, Jr., "Statistics of the recombination of holes and electrons," Phys. Rev. . 87, 5, 835-842 (1952).

[3] K. Graff, *Metal Imputities in Silicon-Device Fabrication* (Springer, 1995), p. 14.

[4] H. Habenicht, M. C. Schubert, and W. Warta, "Imaging of chromium point defects in p-type silicon," J. Appl. Phys. **108**, 034909 (2010).

[5] S. Rein, T. Rehrl, W. Warta, and S. W. Glunz, "Lifetime spectroscopy for defect characterization: Systematic analysis of the possibilities and restrictions," J. Appl. Phys. **91**, 2059-2070 (2002).

[6] J. D. Murphy, K. Bothe, R. Krain, V. V. Voronkov, and R. J. Falster, "Parametrisation of injection-dependent lifetime measurements in semiconductors in terms of Shockly-Read-Hall statistics: An application to oxide precipitates in silicon," J. Appl. Phys. **111**, 113709 (2012).

[7] J. D. Murphy, R. E. McGuire, K. Bothe, V. V. voronkov, and R. J. Falster, "Minority carrier lifetime in silicon photovoltaics: The effect of oxygen precipitation," Sol. Energy Mater. Sol. Cells **120**, 402-411 (2014).

[8] J. Linnros, Carrier lifetime measurements using free carrier absorption transients. I. Principle and injection dependence," J. Appl. Phys. **84**, 275-283 (1998).

[9] Linnros, "Carrier lifetime measurements using free carrier absorption transients. II. Lifetime mapping and effects of surface recombination," J. Appl. Phys. **84**, 284-291 (1998).

[10] H. T. Nguyen, F. E. Rougieux, B. Mitchell, and D. Macdonald, "Temperature dependence of the band-band absorption coefficient in crystalline silicon from photoluminescence," J. Appl. Phys. **115**, 043710 (2014).

[11] H. T. Nguyen, S. C. Baker-Finch, and D. Macdonald, "Temperature dependence of the radiative recombination coefficient in crystalline silicon from spectral photoluminescence," J. Appl. Phys. **104**, 112105 (2014).

[12] A. R. Peaker, B. Hamilton, S. Leonard, V. P. Markevich, K. Youssef, and G. Rozgonyi, "Recombination via nano-precipitates...a new mechanism for efficiency loss in solar silicon?" presented at the 40th IEEE Photovoltaics Specialists Conference, Denver, Colorado, 9 June 2014.

[13] K. R. Mcintosh, B. B. Paudyal, and D. H. Macdonald, "Generalized procedure to determine the dependence of steady-state photoconductance lifetime on the occupation of multiple defects," J. Appl. Phys. **104**, 084503 (2008).

[14] R. A. Sinton and A. Cuevas, "Contactless determination of current-voltage characteristics and minoritycarrier lifetimes in semiconductors from quasisteadystate photoconductance data," App. Phys. Lett. **69**, 2510 (1996).

[15] C. Kittel and H. Kroemer, *Thermal Physics*(W.H. Freeman and Company, 1980), pp. 154-188.

[16] S. Rein, *Lifetime Spectroscopy: A Method of Defect Characterization in Silicon for Photovoltaic Applications* (Springer, 2005), pp. 7-46.